New Journal of Physics
The open access journal at the forefront of physics

Deutsche Physikalische Gesellschaft DPG IOP Institute of Physics

OPEN ACCESS

Nonlinear localized states in the vicinity of topological defects in waveguide arrays

To cite this article: Matthias Heinrich *et al* 2010 *New J. Phys.* **12** 113020

View the article online for updates and enhancements.

You may also like

- Formation of discrete solitons as a function of waveguide array geometry under the well-confined mode condition
A Vergara-Betancourt, E Martí-Panameño, A Luis-Ramos et al.
- Equilibria and precession in a uniaxial antiferromagnet driven by the spin Hall effect
Qiao-Hua Li, Peng-Bin He, Meng-Qiu Cai et al.
- Tunable oscillation of discrete solitons triggered by coherent interactions
Fajun Xiao, Peng Zhang, Sheng Liu et al.

This content was downloaded from IP address 18.118.164.42 on 04/05/2024 at 05:33

New Journal of Physics
The open-access journal for physics

Nonlinear localized states in the vicinity of topological defects in waveguide arrays

Matthias Heinrich[1,4], **Robert Keil**[1], **Felix Dreisow**[1], **Andreas Tünnermann**[1,2], **Stefan Nolte**[1,2] **and Alexander Szameit**[1,3]

[1] Institute of Applied Physics, Friedrich-Schiller-Universität Jena, Max-Wien-Platz 1, D-07743 Jena, Germany
[2] Fraunhofer Institute for Applied Optics and Precision Engineering, Albert-Einstein-Straße 7, D-07745 Jena, Germany
[3] Physics Department and Solid State Institute, Technion, 32000 Haifa, Israel
E-mail: heinrich@iap.uni-jena.de

New Journal of Physics **12** (2010) 113020 (11pp)
Received 13 July 2010
Published 10 November 2010
Online at http://www.njp.org/
doi:10.1088/1367-2630/12/11/113020

Abstract. We report on the impact of topological defects on the formation of discrete spatial solitons in waveguide arrays. The influence of defects, i.e. waveguides with a detuned effective refractive index, is well understood within such systems. They have been shown to support linear bound states and thus influence the formation of spatial solitons in the surrounding sites. We show numerically and demonstrate experimentally how the presence of topological defects caused by junctions within the otherwise periodical system also has a strong influence on the surrounding sites.

Contents

[4] Author to whom any correspondence should be addressed.

© IOP Publishing Ltd and Deutsche Physikalische Gesellschaft

1. Introduction

Discrete solitons in arrays of evanescently coupled waveguides [1]–[3] offer a variety of potential applications in integrated optics. One of the most intriguing possibilities is the use of tightly localized solitons to block off certain paths at photonic network junctions [4], enabling nonlinear switching and routing and thus providing essential basic components for optical signal processing. In this context, a knowledge of the influence of those junctions on the formation of solitons in the vicinity is vital for design and optimization. In analogy to conventional defects formed by detuned waveguides, which have been the subject of detailed investigations in recent years (see e.g. [5]–[8]), junctions act as perturbations to the periodicity of the waveguide array and, consequently, can be perceived as so-called topological defects [9]. As proposed in [10] for kinks (junctions with two oblique branches), the similarity between topological and conventional defects may be employed e.g. to mitigate reflections by introducing an appropriate detuning at the pivotal guide [11]. Here, we investigate topological defects imposed by junctions or truncations with respect to their influence on the formation of discrete solitons in the surrounding waveguides.

2. Numerical investigation

To gain insights into the dynamics of soliton formation, we describe the propagation of light with the nonlinear paraxial Schrödinger equation for the normalized field amplitude Φ in the moving frame (i.e. the group velocity is removed by normalization), assuming continuous wave (cw) illumination:

$$[2kn_0\mathrm{i}\partial_z + \partial_x^2 + \partial_y^2 + |\Phi|^2 + 2k^2n_0\Delta n(x, y)]\Phi(x, y, z) = 0. \tag{1}$$

Here, n_0 denotes the bulk refractive index, x, y and z are the transverse and longitudinal coordinates and k is the vacuum wave number. The refractive index profiles (see figure 1(a)) of junctions between M branches of N coupled nonlinear waveguides each are represented by

$$\Delta n(x, y) = G(x - x_{0,0}, y - y_{0,0}) + \sum_{m=1}^{M}\sum_{n=1}^{N} G(x - x_{m,n}, y - y_{m,n}), \tag{2}$$

where

$$G(x, y) = p \cdot \left\{\frac{2}{3}\exp\left[-\left(\frac{x}{w_x}\right)^2 - \left(\frac{y}{w_y}\right)^2\right] + \frac{1}{3}\exp\left[-\left(\frac{x}{w_x}\right)^2 - \left(\frac{y}{2w_y}\right)^2\right]\right\} \tag{3}$$

describes the shape of the individual waveguides [12] and $(x_{m,n}, y_{m,n})$ denote the positions of the respective guides. Using a nonlinear finite element method, stationary solutions of equation (1) were computed according to the separation ansatz $\Phi(x, y, z) = \phi(x, y)\exp(\mathrm{i}\beta z)$. Note that the reference frame moves at a velocity of c/n_0, while the linear waveguide mode has an effective index $n_{\mathrm{eff}} > n_0$. Hence, the eigenvalue β includes a relative wave vector $\beta_0 = k(n_{\mathrm{eff}} - n_0)$. Among the conserved quantities of equation (1) is the total energy flow

$$U = \frac{1}{2k^2n_0n_2}\int\int_{-\infty}^{+\infty} |\Phi|^2\,\mathrm{d}x\,\mathrm{d}y, \tag{4}$$

the dependence of which on β may be investigated to study the system. The nonlinear refractive index is designated n_2. Corresponding to the experimental parameters, we modeled systems

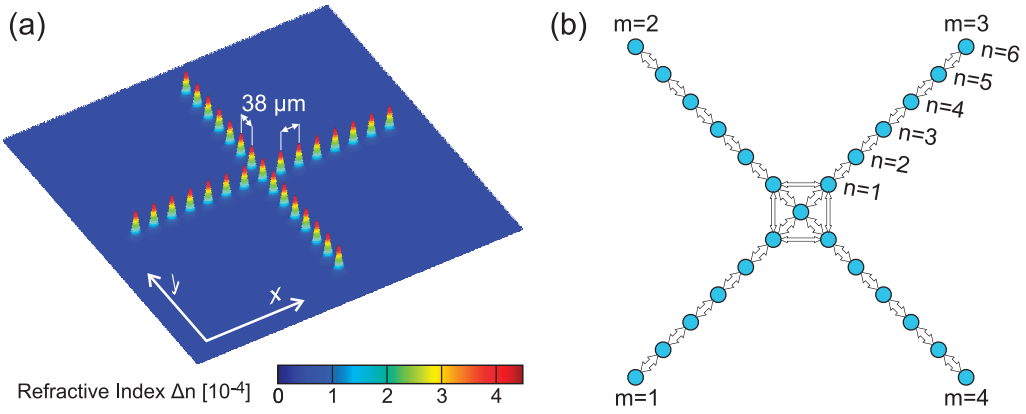

Figure 1. Waveguide array junction with $N = 7$ and $M = 4$ (X junction with seven waveguides per branch). (a) Refractive index profile according to equation (2). (b) Discrete model of the same system corresponding to the coupled mode approximation. The waveguides are represented by circles, while the couplings included are illustrated by arrows. The individual waveguides are labeled with respect to their branch ($m = 1, \ldots, M$) and the distance from the pivotal guide ($n = 1, \ldots, N$); the pivotal guide is designated as $m = n = 0$.

comprising waveguides with an index increase of $p = 4.3 \times 10^{-4}$ and widths $w_x = 6.8\,\mu$m, $w_y = 3.5\,\mu$m separated by a spacing of $38\,\mu$m.

In addition to the continuous approach, the coupled mode approximation [13] was applied (see figure 1(b)), yielding the following set of nonlinear differential equations for the modal amplitudes within the individual waveguides:

$$\mathrm{i}\partial_z \varphi_k + |\varphi_k|^2 \varphi_k + \sum_{\ell \neq k} C_{k,\ell}\, \varphi_\ell = 0. \tag{5}$$

In this context, k is the discrete transverse coordinate and the coefficients $C_{k,\ell} = C_{\ell,k}$ of the symmetric coupling matrix indicate the rate of energy transfer between the waveguides k and ℓ. Due to the approximately exponential dependence of the coupling on the waveguide separation [14], nearest-neighbor coupling (designated C and assumed to be constant throughout the system) is usually sufficient to describe the propagation of light with reasonable accuracy. Despite its limitations, this formalism enables the investigation of the influence of arbitrary couplings for otherwise fixed properties of the system. Here, we consider additional coupling between the first sites of neighboring branches (henceforth termed second-order coupling C_2), which becomes relevant as their separation approaches the pitch within the individual branches. In the discrete model, the normalized total power is given by

$$\widetilde{U} = \sum_{\ell} |\varphi_\ell|^2 \tag{6}$$

and can be plotted over the propagation constant b of stationary solutions $\varphi_n(z) = \phi_n \exp(\mathrm{i}bz)$.

It is instructive to first analyze the impact of three different kinds of perturbations in planar waveguide arrays: a truncation, a waveguide with a higher refractive index than all other guides (positively detuned defect) and a waveguide with a lower refractive index than the other guides (negatively detuned defect). The numerical results obtained from equation (1) are summarized

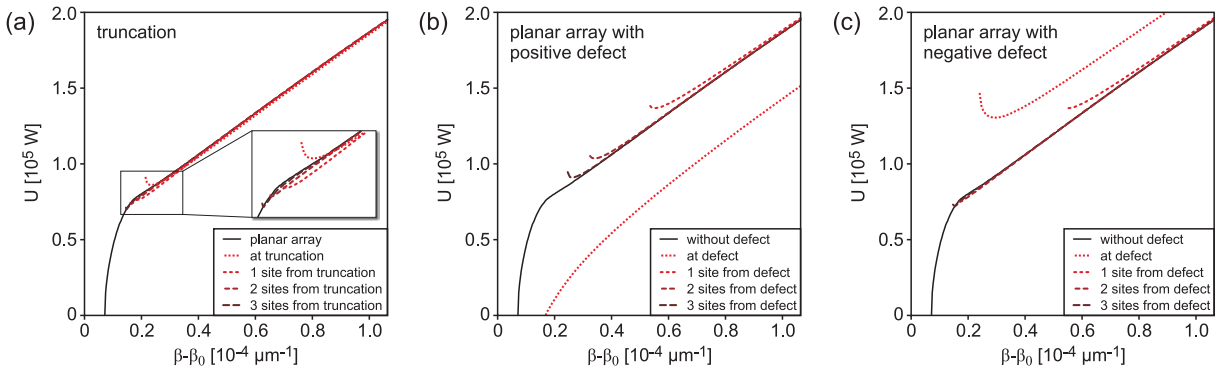

Figure 2. $U(\beta)$-diagrams as obtained from equation (1): (a) a truncated planar array with 13 waveguides, (b) a planar array of 25 waveguides with a positively detuned central waveguide ($p' = 1.025\ p$) and (c) a planar array of 25 waveguides with a negatively detuned central waveguide ($p' = 0.985\ p$). In all diagrams, the $U(\beta)$ graph of an unperturbed planar array of 25 identical waveguides is given as a reference (solid lines).

in figure 2(a). The solid graph shows the unperturbed array with 25 identical waveguides. It exhibits the typical thresholdless behavior, emerging from the β-axis at a certain cutoff propagation constant. Hence, in the absence of defects, stationary solutions exist for all powers. Furthermore, U increases monotonically with β. However, the situation changes when the array is truncated. The pivotal site of this single-branch 'junction', i.e. the outermost waveguide of the array, no longer supports stationary solutions for arbitrary powers. Rather, these so-called surface solitons [15, 16] feature significant power thresholds (dotted line). Nevertheless, the graph still converges toward the unperturbed case for large β. Importantly, such a truncation not only has a local impact, but also induces power thresholds for solitons residing at the adjacent guides (various dashed lines).

In figure 2(b), the $U(\beta)$ graphs for a positively detuned waveguide ($p' = 1.025\ p$) embedded within an otherwise homogeneous array are shown. Such a defect always creates bound states [17]. At the defect guide itself, the cutoff is significantly increased (dotted graph), but solitons still exist for all power levels. In contrast to the truncation, the influence of the detuned waveguide does not subside for large β. This difference becomes clear if one considers that, for the corresponding large powers, the transverse profile of a soliton essentially becomes localized within a single waveguide. Since this mitigates the influence of neighboring guides, the shift along the β-axis introduced by the detuned guide increases and eventually converges toward the value of the detuning. Interestingly, the positive defect imposes power thresholds on the adjacent guides (dashed graphs), similar to the truncation. Solitons centered on the waveguide next to the positive defect exhibit a substantial threshold, much higher than in the waveguide next to a truncation. However, for large β the strongly localized soliton does not 'feel' the defect anymore, so that the $U(\beta)$ graph eventually converges to the unperturbed planar case for large β. In a similar vein, the threshold power decreases for solitons residing on waveguides further away from the pivotal guide, and for high β the $U(\beta)$ graph approaches the one of the unperturbed array. The situation for a negatively detuned waveguide ($p' = 0.985\ p$) is depicted in figure 2(c). Here, solitons centered on the defect exhibit a power threshold. Compared to the unperturbed array, the cutoff is also increased, and for high β the shift of

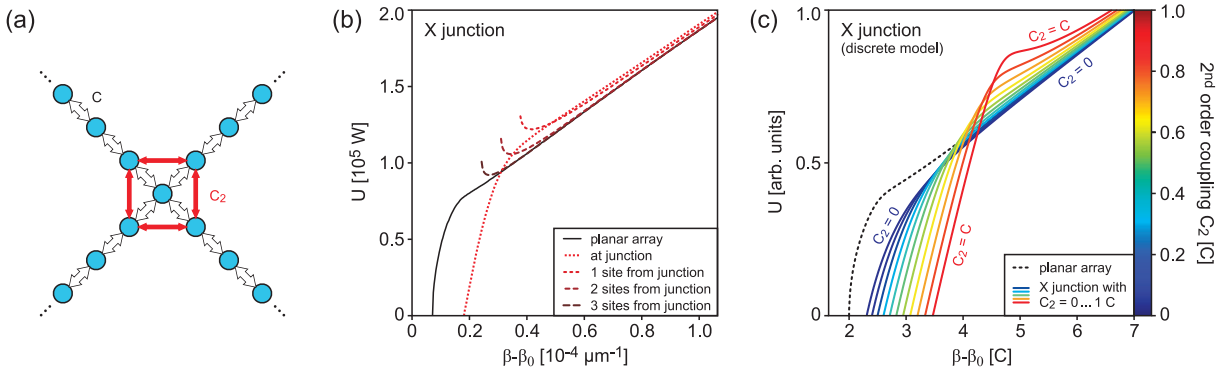

Figure 3. (a) Sketch of an X junction with second-order coupling around the pivotal guide, with the circles representing the waveguides. When using the discrete model (5), the coupling constant, visualized with arrows, has to be chosen manually. (b) $U(\beta)$-diagrams as obtained from equation (1) for an X junction with seven waveguides per branch. (c) $U(\beta)$-diagrams calculated using the coupled mode approximation equation (5). Dashed line: an unperturbed planar array. Solid lines: a pivotal guide of X junctions with varying degrees of second-order coupling ($C_2 = 0, \ldots, C$ in steps of $0.1\,C$).

$U(\beta)$ again approaches the value of the detuning. The impact of the defect is still evident in the neighboring guide, where solitons exhibit a similar power threshold, but rapidly decreases for waveguides further away. Additionally, for high β the $U(\beta)$ graphs of these guides converge to the one of the unperturbed array. The impact of a topological defect in an X junction ($M = 4$) with $N = 7$ waveguides per branch is illustrated in figure 3. When calculating the power for solitons centered on this guide, one finds the cutoff shifted toward larger β (figure 3(b)). While the monotonic dependence of $U(\beta)$ is preserved, the graph is deformed such that it intersects with the unperturbed case. Consequently, solutions with propagation constants above this intersection carry larger powers than their counterparts in an unperturbed array. At large β, the graph eventually converges to the corresponding graph of the unperturbed case, since the solitons are strongly localized, rendering the influence of the neighboring guides negligibly small. Numerical investigations of the coupled mode approximation equation (5) of this system show that the specific behavior at intermediate values of β is chiefly determined by the second-order coupling around the pivotal guide (figure 3(a)). In the ideal case of $C_2 = 0$, the graph quickly converges toward the unperturbed planar array (figure 3(c)). As C_2 increases, the shift of the cutoff β becomes more prominent. Interestingly, at intermediate values of β, U may increase significantly above the power carried by the corresponding solitons in the unperturbed planar array. Although in practice second-order coupling in the vicinity of the junction cannot be tuned independently, both C and C_2 follow the same exponential dependence on the distance between the coupling waveguides [14]. The fixed ratio of waveguide separations ($d_2 = \sqrt{2}\,d$ for a symmetric X junction) consequently allows a certain scaling of the ratio C_2/C with the pitch of the system.

The influence of the junction becomes even more apparent at the neighboring guides where the presence of the topological defect leads to power thresholds on soliton formation (various dashed graphs in figure 3(b)). Certain minimum powers are required for the existence of solitons and the corresponding cutoffs values of β are increased accordingly. This influence abates with

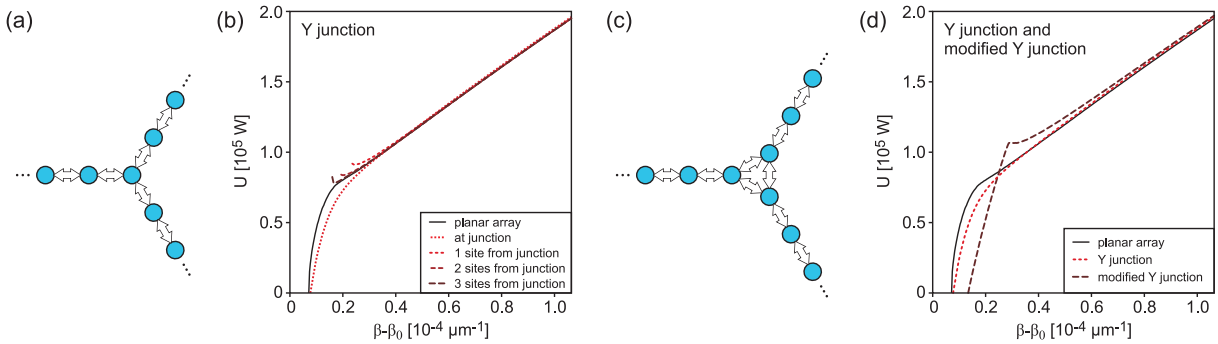

Figure 4. (a) Schematic diagram of a common Y junction. (b) $U(\beta)$-diagrams for a Y junction with seven waveguides per branch. (c) Schematic diagram of a modified Y junction with an extended pivotal region. (d) $U(\beta)$-diagrams for exciting the pivotal sites in (a) and (b) (dashed graphs) compared to the unperturbed planar array (solid graph). The $U(\beta)$-diagrams in (b) and (d) were obtained from equation (1).

increasing distance to the pivotal guide, and for increasing powers the graphs again converge toward the unperturbed case.

In a Y junction ($M = 3$, $N = 7$), sketched in figure 4(a), the topological defect is less pronounced, owing to fewer branches. Nevertheless, in figure 4(b) the basic features of the X junction (compare figure 3(b)) are reproduced. Interestingly, in a modified Y junction (sketched in figure 4(c)), the impact of the topological defect on the pivotal guide is even more pronounced. The cutoff is larger, and the soliton power crosses the one for the unperturbed array, and even exhibits a quite sharply pronounced local maximum, before it eventually approaches the one of the unperturbed array for large β. In general, the $U(\beta)$ dependence closely resembles the behavior reported in waveguide arrays with intermediate dimensionality [18]. This clearly shows how the impact of topological defects can be strongly enhanced with a minor modification of the geometry of the setting.

By comparing the results for the X junction (figure 3) and the Y junction (see figure 4) with the conventional defects (figure 2), one finds various related features. It is evident that the topological defects act in a similar fashion to positive defects: solitons centered on the pivotal guide bifurcate from a linear mode, i.e. they exist for all power levels. Furthermore, solitons centered on neighboring waveguides exhibit a power threshold, which decreases with increasing distance from the pivotal guide. The strength of a junction's topological defect is determined by the number M of its branches. However, there is one important distinction: for high β, the impact of topological defects vanishes, whereas a real defect persists.

3. Experimental results

For our experiments, we used the femtosecond laser direct inscription technique [19] to fabricate junctions with six waveguides per branch within fused silica. The fabrication process is shown schematically in figure 5, and specific writing parameters are discussed in [20]. A waveguide separation of 38 μm was chosen in order to avoid reflections from the end of the branch during the propagation distance of 105 mm. A T:sapphire laser system (Spectra Physics

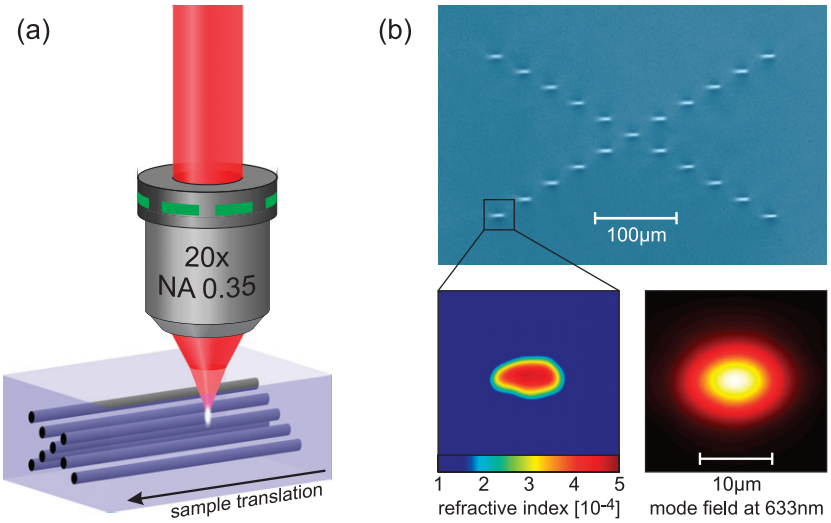

Figure 5. (a) Schematic representation of the femtosecond laser direct writing method. (b) Micrograph of the fabricated X junction, exemplary refractive index profile and corresponding mode field of a single waveguide measured at 633 nm.

Tsunami/Spitfire), delivering 200 fs pulses at a wavelength of 800 nm with a repetition rate of 1 kHz, was used to excite individual waveguides via a 5× microscope objective. Subsequently, the discrete diffraction patterns at different excitation powers were observed by imaging the sample end facet onto a CCD camera.

Generally, the power required to achieve localization within the excited guide decreased for the pivotal sites and increased for the neighbors with respect to an unperturbed planar array. As expected from the numerical analysis, the impact of the topological defect is most pronounced for the X junction. Light injected into the pivotal guide itself remains localized independent of the excitation power (left column of figure 6). It follows that the topological defect is sufficiently strong to support a tightly localized linear mode indistinguishable from the solitons forming at higher powers. In contrast, an excitation of the guide next to the junction (middle column) at low powers mainly spreads into the far side of the branch due to reflection at the topological defect. At intermediate powers, phase matching between the excited guide and the pivotal guide occurs, causing the intensity maximum to shift to the pivotal guide, until at high powers the light can overcome the attraction of the defect state and finally stays trapped in the excited guide. Light injected into the waveguide two sites away from the pivotal site of the X junction spreads across the excited branch, as well as across the junction into the first guides of the other branches. Similar to the localization behavior in the unperturbed planar array, an increase of power leads to a continuous contraction until finally all light remains localized in the excited guide (right column).

The observations for the Y junction are summarized in figure 7. In contrast to the X junction, the topological defect does not support a strongly localized linear mode at the pivotal guide (left column). The symmetry of the arrangement is broken due to the ellipticity of the waveguides, so that the light mostly diffracts into one branch of the junction when light is launched into the pivotal guide. At increasing input power, light gradually localizes in the excited site, and eventually forms a strongly confined soliton. When injecting the light into the

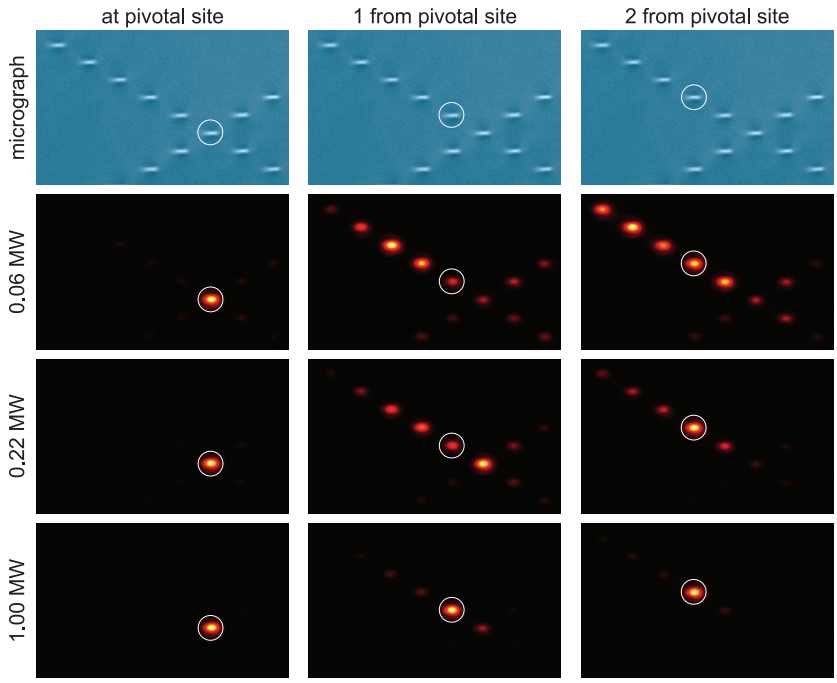

Figure 6. Observed diffraction patterns of the X junction at 800 nm for excitation at the pivotal guide (first column), one site from the pivotal guide (second column) and two sites from the pivotal guide (third column). The first row: micrographs of the relevant region of the system; the second row: 0.06 MW; the third row: 0.22 MW; the fourth row: 1.00 MW peak power. White circles mark the excited waveguides.

neighboring waveguide, at low input power light is reflected from the topological defect (middle column). For intermediate powers, the nonlinear phase matching augments the attraction of the topological defect, so that the maximum light intensity is shifted into the pivotal guide. At high power, eventually a localized soliton is formed. Exciting the waveguide two sites away from the pivotal guide (right column) at low power yields an asymmetric diffraction pattern, since light is reflected by the junction. This effect persists even at intermediate powers, where a slight contraction of the diffraction pattern is already observed. At high powers, the soliton is eventually localized within the excited guide. Note that compared to the X junction, the injected light contracts into the excited guide at lower powers for all neighboring sites.

In figure 8, a summary of the measured degree of localization as a function of the input power is shown. When launching light into an unperturbed array, light gradually localizes in the excited lattice site with increasing input power. If the array is truncated, launching the light into the boundary waveguide results in an enhanced delocalization at low powers due to repulsion of the array boundary [21]. However, light localizes at high power in a similar fashion as in the unperturbed array. The plot for the pivotal guide of the Y junction shows a slight enhancement compared to the unperturbed planar array, which can be attributed to the comparably small topological defect. In contrast, in the X junction, the topological defect is much more pronounced and consequently supports a strongly localized linear mode, which yields high degrees of localization even at low powers. Hence, at high powers localization increases only slightly.

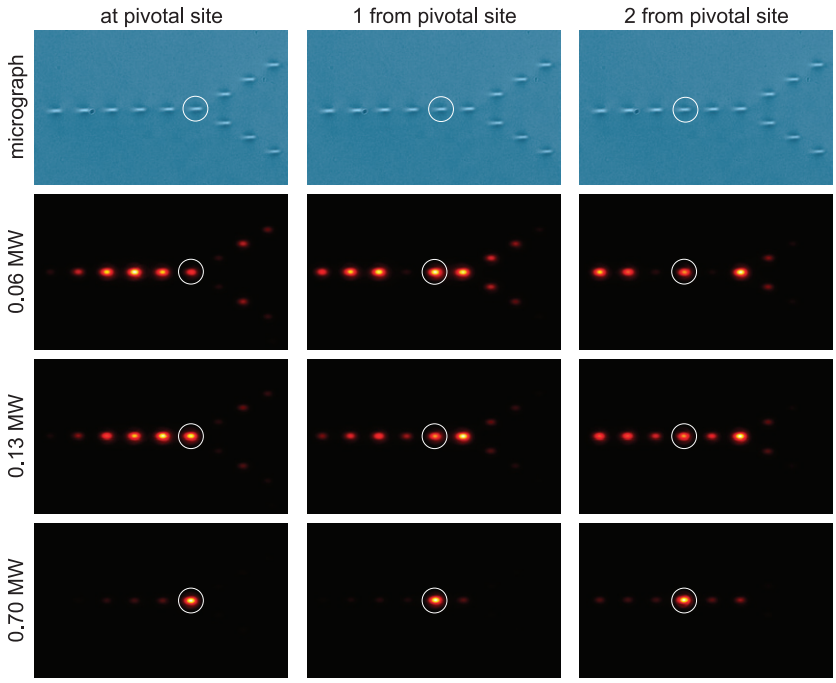

Figure 7. Observed diffraction patterns of the Y junction at 800 nm for excitation at the pivotal guide (first column), one site from the pivotal guide (second column) and two sites from the pivotal guide (third column). The first row: micrographs of the relevant region of the system; the second row: 0.06 MW; the third row: 0.13 MW; the fourth row: 0.70 MW peak power. White circles mark the excited waveguides.

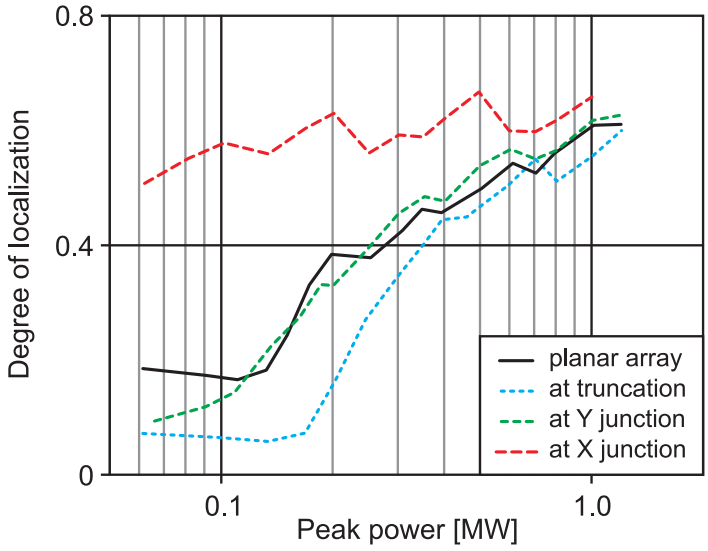

Figure 8. Measured power dependence of the degree of localization at the pivotal sites of truncation, Y and X junctions (various dashed graphs) compared to the unperturbed planar array (solid graph).

4. Conclusion

In conclusion, we have demonstrated numerically and verified experimentally that topological defects influence the formation of solitons in close resemblance to defects represented by detuned waveguides. Junctions with an increased number of neighbors around the pivotal guide act as positive defects, while truncations can be interpreted as negative defects. In contrast to detuning defects, the influence of topological defects on solitons centered on the pivotal guide vanishes for large values of the propagation constant β. Topological defects of sufficient strength support strongly localized linear modes. Solitons centered on neighboring waveguides exhibit a power threshold. Nevertheless, tightly localized solitons emerge as the influence of topological perturbations becomes negligible for sufficiently high powers. In order to minimize the impact of topological defects and hence the power requirements for soliton formation in the adjacent sites, the number of branches per junction should be as close as possible to the unperturbed case of the planar array. Consequently, Y junctions constitute the building block of choice for array-based photonic networks. We believe these findings will pave the way for future developments in utilizing solitons as blockers in array junctions [22] for two- and even three-dimensional all-optical routing and switching schemes.

Acknowledgments

Financial support from the Deutsche Forschungsgemeinschaft (the research unit FG 532 'Nonlinear spatio-temporal dynamics in dissipative and discrete optical systems' and Leibniz program) and the German Academy of Science Leopoldina (grant no. LPDS 2009-13) is gratefully acknowledged.

References

[1] Christodoulides D and Joseph R 1988 Discrete self-focusing in nonlinear arrays of coupled waveguides *Opt. Lett.* **13** 794–6
[2] Eisenberg H, Silberberg Y, Morandotti R, Boyd A and Aitchison J 1998 Discrete spatial optical solitons in waveguide arrays *Phys. Rev. Lett.* **81** 3383–6
[3] Fleischer J, Segev M, Efremidis N and Christodoulides D 2003 Observation of two-dimensional discrete solitons in optically induced nonlinear photonic lattices *Nature* **422** 147–50
[4] Christodoulides D and Eugenieva E 2001 Blocking and routing discrete solitons in two-dimensional networks of nonlinear waveguide arrays *Phys. Rev. Lett.* **87** 233901
[5] Peschel U, Morandotti R, Aitchison J, Eisenberg H and Silberberg Y 1999 Nonlinearly induced escape from a defect state in waveguide arrays *Appl. Phys. Lett.* **75** 1348–50
[6] Fedele F, Yang J and Chen Z 2005 Defect modes in one-dimensional photonic lattices *Opt. Lett.* **30** 1506–8
[7] Makasyuk I, Chen Z and Yang J 2006 Band-gap guidance in optically induced photonic lattices with a negative defect *Phys. Rev. Lett.* **96** 223903
[8] Szameit A, Kartashov Y V, Heinrich M, Dreisow F, Pertsch T, Nolte S, Tünnermann A, Lederer F, Vysloukh V A and Torner L 2009 Observation of two-dimensional defect surface solitons *Opt. Lett.* **34** 797–9
[9] Miroshnichenko A, Molina M and Kivshar Y 2007 Localized modes and bistable scattering in nonlinear network junctions *Phys. Rev.* E **75** 046602
[10] Christodoulides D and Eugenieva E 2001 Minimizing bending losses in two-dimensional discrete soliton networks *Opt. Lett.* **26** 1876–8

[11] Eugenieva E, Efremidis N and Christodoulides D 2001 Design of switching junctions for two-dimensional discrete soliton networks *Opt. Lett.* **26** 1978–80
[12] Heinrich M, Kartashov Y V, Szameit A, Dreisow F, Keil R, Nolte S, Tünnermann A, Vysloukh V A and Torner L 2009 Observation of two-dimensional coherent surface vector lattice solitons *Opt. Lett.* **34** 1624
[13] Jones A 1965 Coupling of optical fibers and scattering in fibers *J. Opt. Soc. Am.* **55** 261–71
[14] Szameit A, Dreisow F, Pertsch T, Nolte S and Tuennermann A 2007 Control of directional evanescent coupling in fs laser written waveguides *Opt. Express* **15** 1579–87
[15] Makris K, Suntsov S, Christodoulides D and Stegeman G 2005 Discrete surface solitons *Opt. Lett.* **30** 2466–8
[16] Suntsov S, Makris K, Christodoulides D, Stegeman G, Hache A, Morandotti R, Yang H, Salamo G and Sorel M 2006 Observation of discrete surface solitons *Phys. Rev. Lett.* **96** 063901
[17] Trompeter H, Peschel U, Pertsch T, Lederer F, Streppel U, Michaelis D and Braeuer A 2003 Tailoring guided modes in waveguide arrays *Opt. Express* **11** 3404–11
[18] Szameit A, Kartashov Y V, Dreisow F, Heinrich M, Pertsch T, Nolte S, Tünnermann A, Vysloukh V A, Lederer F and Torner L 2009 Soliton excitation in waveguide arrays with an effective intermediate dimensionality *Phys. Rev. Lett.* **102** 063902
[19] Itoh K, Watanabe W, Nolte S and Schaffer C 2006 Ultrafast processes for bulk modification of transparent materials *MRS Bull.* **31** 620–5
[20] Szameit A, Burghoff J, Pertsch T, Nolte S, Tuennermann A and Lederer F 2006 Two-dimensional soliton in cubic fs laser written waveguide arrays in fused silica *Opt. Express* **14** 6055–62
[21] Molina M, Vicencio R and Kivshar Y 2006 Discrete solitons and nonlinear surface modes in semi-infinite waveguide arrays *Opt. Lett.* **31** 1693–5
[22] Keil R, Szameit A, Dreisow F, Heinrich M, Nolte S and Tünnermann A 2009 All-optical routing and switching in two-dimensional waveguide arrays *CLEO/Europe—IQEC Conf.* paper CD9.1 (invited)